ÉCOLE POLYTECHNIQUE FÉDÉRALE DE LAUSANNE

MATHICSE

Mathematics Institute of Computational Science and Engineering

School of Basic Sciences - Section of Mathematics

MATHICSE Technical Report

Nr. 20.2012

June 2012

Numerical simulation of left ventricular assist device implantations: comparing the ascending and descending aorta cannulations

J. Bonnemain, C. Mallossi, M. Lesinigo, S. Deparis, A. Quarteroni, L. von Segesser

http://mathicse.epfl.ch

Phone: +41 21 69 37648

Address:
EPFL - SB - MATHICSE (Bâtiment MA)
Station 8 - CH-1015 - Lausanne - Switzerland

Fax: +41 21 69 32545

Numerical simulation of left ventricular assist device implantations: comparing the ascending and the descending aorta cannulations

Jean Bonnemain[a,b,*], A. Cristiano I. Malossi[a], Matteo Lesinigo[a], Simone Deparis[a], Alfio Quarteroni[a,c], Ludwig K. von Segesser[b]

[a] *CMCS, Chair of Modelling and Scientific Computing, MATHICSE, Mathematics Institute of Computational Science and Engineering, EPFL, École Polytechnique Fédérale de Lausanne, Station 8, CH-1015, Lausanne, Switzerland*
[b] *Department of Surgery, University Hospital of Lausanne (CHUV), Rue du Bugnon 21, CH-1011, Lausanne, Switzerland*
[c] *MOX, Modeling and Scientific Computing, Department of Mathematics, Politecnico di Milano, Via Bonardi 9, Milan, Italy*

Abstract

In this work we present numerical simulations of continuous flow left ventricle assist device implantation with the aim of comparing difference in flow rates and pressure patterns depending on the location of the anastomosis and the rotational speed of the device. Despite the fact that the descending aorta anastomosis approach is less invasive, since it does not require a sternotomy and a cardiopulmonary bypass, its benefits are still controversial. Moreover, the device rotational speed should be correctly chosen to avoid anomalous flow rates and pressure distribution in specific location of the cardiovascular tree. With the aim of assessing the differences between these two approaches and device rotational speed in terms of flow rate and pressure wave forms, we set up numerical simulations of network of one-dimensional models where we account for the presence of an outflow cannula anastomosed to different locations of the aorta. Then, we use the resulting network to compare the results of the two different cannulations for several stages of heart failure and different rotational speed of the device. The inflow boundary data for the heart and the cannulas are obtained from a lumped parameters model of the entire circulatory system with an assist device, which is validated with clinical data. The results show that ascending and descending aorta cannulations lead to similar wave forms and mean flow rate in all the considered cases. Moreover, regardless of the anastomosis region, the rotational speed of the device has an important impact on wave profiles; this effect is more pronounced at high RPM.

Keywords: Left ventricular assist device, geometrical multiscale modeling, blood flow models, wave propagation, hemodynamics.

1. Introduction

The implant of a ventricular assist device (VAD) has become a common therapeutic approach for treating heart failure, especially because of the lack of donors and to the raising number of patients presenting terminal heart failure[1,2]. At the early stage the use of a VAD was indicated for patients on the transplantation waiting list (*bridge to transplantation*[3]) and for patients with a temporary need of circulatory support (*bridge to recovery*[4]).

With the development of more effective devices and the improvement of the clinical experience, the indication for the procedure has widen and it is now proposed to patients who are ineligible for transplantation (*destination therapy*[5]) and also in situations of extreme emergency (*bridge to decision*[6]).

When using a continuous-flow left ventricular assist device (LVAD), such as the HeartMate II® (Thoratec Corporation[a]), the outflow cannula is usually anastomosed to the ascending aorta (AA). However, other devices such as the Jarvik 2000 FlowMaker® (Jarvik Heart Inc.[b]) allow to perform the anastomosis to the descending aorta (DA). The latter procedure is less invasive for the patient as it consists in a left thoracotomy without a cardiopulmonary bypass (CPB)[7] and avoids the adverse effects of the CPB and the sternotomy, especially in the case of patients who are critically ill and already had multiple median sternotomy[8].

Nevertheless the beneficial effect of this procedure is still controversial. For instance, Litwak and co-workers[9] performed *in vivo* experiments showing that DA anastomosis induces a significant lower flow rate in the aortic

*Corresponding author
Email addresses: jean.bonnemain@epfl.ch (Jean Bonnemain), cristiano.malossi@epfl.ch (A. Cristiano I. Malossi), matteo.lesinigo@epfl.ch (Matteo Lesinigo), simone.deparis@epfl.ch (Simone Deparis), alfio.quarteroni@epfl.ch (Alfio Quarteroni), ludwig.von-segesser@chuv.ch (Ludwig K. von Segesser)

[a] http://www.thoratec.com.
[b] http://www.jarvikheart.com.

arch and an abnormal flow pattern, such as turbulent regions. This has been further confirmed in Litwak et al.[10] through *in vitro* experiments where the combined ejection of the DA anastomosed cannula and the heart induced regions of stagnation and turbulence which could potentially have clinical consequences[11]. Moreover Nawata and co-workers[12] reported adverse clinical effects in patients with DA anastomosis, especially thromboembolic events. In addition, the numerical results provided by Bazilev et al.[13] indicate deficiencies associated with the implantation of the LVAD in the descending branch of the thoracic aorta, specifically, blood flow stagnation, abnormally high mean wall shear stress in the vicinity of the implant, and abnormally low and highly oscillatory wall shear stress in the aortic arch.

However, the reliability of DA anastomosis with the Jarvik 2000 FlowMaker® device has been demonstrated clinically by Frazier et al.[14]. Furthermore, Tuzun et al.[15] showed that myocardial blood flow is not adversely affected by the outflow-graft anastomosis and Ghodsizad et al.[16] reported the advantages of DA anastomosis without CPB; both studies were conducted on animals.

Few studies were performed by mathematical and numerical models to compare the different sites of outflow cannula anastomosis[17,18,19]. Moreover, at the best of our knowledge, only Kar et al.[20] compared the AA and DA configurations, highlighting the presence of stagnation zones in the aortic arch, especially in the DA configuration.

On a slightly different context, another relevant aspect that should be addressed to help physicians improving the correct tuning of the device is the assessment of the response of the cardiovascular system to the rotational speed of the device itself. Recent studies show that variable pump speed is beneficial, especially for outpatient and for exercise[21,22].

Consequently, in this work we aim to:

- develop a new mathematical multiscale framework for assessing the response of the cardiovascular response to the implant of a LVAD;
- assess possible differences in flow rates and pressure patterns depending on the location of the anastomosis;
- assess possible differences in flow rates and pressure patterns depending on rotational speed of the device.

A critical point of the numerical models is the choice of a suitable set of boundary conditions to correctly impose the flow rates provided by the device and by the heart. Up to now, experimental flow rates (either from humans or animals) have been applied as boundary data at the root of the aortic arch, while experimental or extrapolated data have been used as inflow conditions for the anastomosed cannula of the LVAD. Although these methods allow a rough estimation of flows, they do not take into account the fact that the flow rate prescribed by the LVAD depends on the pressure difference across the device and therefore on the left ventricle pressure which is determined by the cardiac function.

To overcome these limitations, in this work we set up a geometrical multiscale model based on the algorithms developed in Malossi et al.[23,24] that:

1. simulates different stages of heart failure;
2. takes into account the interaction of a continuous-flow LVAD with the cardiovascular system (including different rotational speeds and the effects of autoregulation);
3. allows the evaluation of flow rate and pressure at different location of the cardiovascular system;
4. evaluates qualitatively and quantitatively differences between AA and DA anastomosis.

The main ingredient of our geometrical multiscale model is a network of one-dimensional (1-D) models[25], which provides a detailed description of the pulse wave propagation along the arterial tree. The network is terminated by lumped parameters windkessel models to account for the peripheral circulation. Inflow boundary conditions are determined a priori by using the global circulation lumped parameters model[26], which has been slightly modified to account for the presence of the LVAD.

This work is organized as follows. In Section 2 we briefly describe the geometrical multiscale model and the lumped parameters model. Then, in Section 3 we use the lumped parameters model to generate the inflow boundary conditions at the cannula for the geometrical multiscale model, whose results are presented in Section 4. Finally, the main conclusions of our investigation are drawn in Section 6.

2. Models and methods

In this section we summarize the main components of our geometrical multiscale model. First we introduce the network of 1-D models describing the global arterial circulation proposed by Reymond et al.[25], that has been slightly modified to account for the presence of the two aforementioned cannula configurations. Then, we recall from the work of Ursino et al.[26] a lumped parameters model for the global circulation, which is used to generate the inflow boundary data for the geometrical multiscale problem.

To have comparable results between the two cannulation possibilities, we decided to use the parameters of only one device, the Thoratec HeartMate II®, although this device is neither designed nor approved for a DA cannulation.

2.1. 1-D FSI model for the global arterial circulation

Numerical simulations of the cardiovascular system using a collection of simple distributed 1-D fluid-structure interaction (FSI) models have proven to be able to provide useful information under physiological and pathophysiological conditions. In particular, they give insight

about the main characteristics of the flow and the interplay among physical phenomena taking place in the systemic arteries[27,28,29,30,31,32,33].

2.1.1. Equations and numerical approximation

The 1-D FSI model is derived from the incompressible Navier–Stokes equations by introducing some simplifying hypotheses on the behavior of the flow quantities over the cross-section of the artery. Being $z \in [0, L]$ the axial coordinate, with L the length of the vessel, the resulting governing equations are

$$\begin{cases} \dfrac{\partial A}{\partial t} + \dfrac{\partial Q}{\partial z} = 0 \quad \text{in } (0,L)\times(0,T], \\ \dfrac{\partial Q}{\partial t} + \dfrac{\partial}{\partial z}\left(\alpha_{\mathrm{F}}\dfrac{Q^2}{A}\right) + \dfrac{A}{\rho_{\mathrm{F}}}\dfrac{\partial P}{\partial z} \\ \qquad\qquad +\kappa_{\mathrm{F}}\dfrac{Q}{A} = 0 \quad \text{in } (0,L)\times(0,T], \end{cases} \tag{1}$$

where α_{F} and κ_{F} are the Coriolis and friction coefficients, respectively, whose definitions are given in Malossi et al.[24], A is the cross-sectional area, Q the volumetric flow rate, and P the average pressure. The fluid problem (1) is coupled with the 1-D structural model through the pressure-area relation

$$P = \psi(A) = P_{\mathrm{ext}} + \hat{\psi}(A) + \tilde{\psi}(A) \quad \text{in } (0,L)\times(0,T], \tag{2}$$

being P_{ext} a reference pressure, i.e., the pressure level at which the vessel area A is equal to the reference area A^0, and

$$\hat{\psi}(A) = \beta_{\mathrm{S}}\left(\sqrt{\frac{A}{A^0}} - 1\right), \qquad \tilde{\psi}(A) = \gamma_{\mathrm{S}}\left(\frac{1}{A\sqrt{A}}\frac{\partial A}{\partial t}\right),$$

with

$$\beta_{\mathrm{S}} = \sqrt{\frac{\pi}{A^0}}\frac{h_{\mathrm{S}}E_{\mathrm{S}}}{1-\nu_{\mathrm{S}}^2}, \qquad \gamma_{\mathrm{S}} = \frac{T_{\mathrm{S}}\tan\phi_{\mathrm{S}}}{4\sqrt{\pi}}\frac{h_{\mathrm{S}}E_{\mathrm{S}}}{1-\nu_{\mathrm{S}}^2},$$

being h_{S} the wall thickness, T_{S} the wave characteristic time, and ϕ_{S} the viscoelastic angle. The functions $\hat{\psi}$ and $\tilde{\psi}$ in (2) account for the elastic and viscoelastic response of the vessel wall. If needed, problem (1) is closed by a proper set of initial and boundary conditions. The latter can be either inflow and outflow boundary data or coupling conditions with other models, as we detail in Section 2.1.3.

From the numerical viewpoint, the 1-D FSI problem is solved by using an operator splitting technique based on an explicit second order Taylor–Galerkin discretization, where the solution of the problem requires two steps: the first one corresponds to the solution of a purely elastic problem, while the second one provides a viscoelastic correction. The spatial discretization is accomplished using $\mathbb{P}1$ finite elements. For more details see Malossi et al.[24].

2.1.2. Human arterial tree model with cannula

To model the global circulation we use the data of the arterial network provided in Reymond et al.[25] (Figure 2 and Table 2), in which the entire arterial network is divided in many small anatomical arterial segments. More precisely, the model is composed by 103 elements, i.e., 24 elements for the aorta, 4 for the coronary system, 51 for the cerebral system, 10 for the upper limbs, and 14 for the lower limbs. It also includes all the values of the parameters required to describe the blood flow, such as the geometrical properties of the vessels (length and proximal/distal areas) and the data for the terminals, which are modeled as three-element windkessel elements. These values have been obtained both from *in vivo* measurements and averaged literature data. The presence of the venous circulation is taken into account by imposing a constant pressure of 5 mmHg on the distal side of each windkessel terminal, i.e., $P_{\mathrm{v}} = 5$ mmHg (see Malossi et al.[24], Figure 7). Regarding the parameters of the wall, since we use a different model, we estimate these values from other sources, as described in Malossi et al.[24].

To account for the presence of the LVAD the global network of 1-D arteries is extended by including an additional segment representing the cannula. As discussed in the introduction, the position of the cannula depends on the chosen approach for the anastomosis. Following the same numeration in Reymond et al.[25] (Figure 2 and Table 2), in the AA configuration the cannula is connected in the middle of the segment 95 (ascending aorta 2), while in the DA configuration it is attached at the junction between segments 18 (thoracic aorta A) and 27 (thoracic aorta B). The end of the outflow cannula of the LVAD is modeled as a stiffer 1-D element (Young modulus $E_{\mathrm{S}} = 4$ MPa) and a diameter of 16 mm as reported by the manufacturer. The inflow boundary data for the cannula are computed by using the lumped parameters model by Ursino et al.[26], as described in Section 2.2.

2.1.3. Interface conditions for the network of models

The solution of the global network of 1-D models is addressed in detail in a previous work of Malossi et al.[24]. We consider a general network of 1-D models connected by $\mathcal{C}$ coupling nodes: at each c-th coupling node we impose the conservation of mass and the continuity of mean pressure as

$$\begin{cases} \displaystyle\sum_{i=1}^{\mathcal{I}_c} Q_{c,i} = 0, \\ P_{c,1} - P_{c,i} = 0, \qquad i = 2,\dots,\mathcal{I}_c, \end{cases} \tag{3}$$

where $\mathcal{I}_c$ is the number of interfaces connected by the c-th coupling node, $c = 1,\dots,\mathcal{C}$. From the numerical viewpoint, the global interface problem is written in a residual formulation and solved by Newton or inexact-Newton methods, where the Jacobian matrix is either computed analytically, by solving the tangent problem associated to each model, or approximated with finite difference. To

avoid the recomputation of the Jacobian matrix at each iteration, a Broyden method is used[24].

2.2. Lumped parameters model for the cannula inflow boundary conditions

Zero-dimensional (0-D) (or lumped or compartmental models) usually provide averaged spatial information about the fundamental variables (pressure, flow, and volume) of the compartment (organ, vessel or part of vessel) of interest at any instant in time, differentiating themselves from higher dimensional models that are also able to capture the spatial variation of these parameters. They are particularly appreciated in the description of complex multi-compartmental systems as they are easy to develop and prototype, fast to solve and may be refined by adding equations for second-order effects and nonlinearities. Usually, lumped parameter models consist of differential algebraic equations describing the conservation of mass and momentum which are complemented by a pressure-volume relation[34,35,36,37]. Lumped models have been extensively applied for modeling the cardiovascular system[26,31,38]. For a recent review on lumped parameters models for cardiovascular problems see Shi et al.[39] and references therein.

2.2.1. Model description

The lumped description of the cardiovascular network is obtained extending the model of Ursino et al.[26] by including a compartment representing the LVAD. Ursino model was developed to provide a lumped mathematical description of the whole cardiovascular system accounting also for autoregulation and therefore constitute a suitable basis for our analysis. The model includes an elastance variable description of the left and right heart, the splanchnic and extrasplanchnic systemic circulation, the pulmonary circulations, the afferent carotid baroreceptor pathway, the sympathetic and vagal efferent activities, and the action of several effector mechanisms. A sketch of the model is depicted in Figure 1. The vascular compartments are modeled by the classical basic $\mathcal{L}$-circuit equivalent equations, derived by linearizing system (1)[40]. The resulting equations relate the volume of the compartment V_{C}, the inlet and outlet volumetric flow rate Q_{in} and Q_{out}, and the inlet and outlet pressure P_{in} and P_{out}. The mass conservation reads

$$\frac{\mathrm{d}V_{\mathrm{C}}(t)}{\mathrm{d}t} = Q_{\mathrm{in}}(t) - Q_{\mathrm{out}}(t), \tag{4}$$

while the momentum conservation is given by

$$P_{\mathrm{in}}(t) - P_{\mathrm{out}}(t) = R_{\mathrm{C}}\, Q_{\mathrm{out}}(t) + L_{\mathrm{C}}\, \frac{\mathrm{d}Q_{\mathrm{out}}(t)}{\mathrm{d}t}, \tag{5}$$

where R_{C} denotes the hydraulic resistance of the compartment and L_{C} the inertance of the flow. Equations (4) and (5) are complemented by a pressure-volume relation by mean of a compliance C_{C}, namely

$$\frac{\mathrm{d}V_{\mathrm{C}}(t)}{\mathrm{d}t} = C_{\mathrm{C}} \frac{\mathrm{d}P_{\mathrm{in}}(t)}{\mathrm{d}t}.$$

Table 1: List of the four parameters calibrated to account for the two heart failure levels (MHF and SHF). The values of the parameters for the HH are the same as those given in Ursino et al.[26].

Parameter[a]	HH	MHF	SHF
$E_{\mathrm{max,lv}}$	2.950	0.800	0.200
$E_{\mathrm{max}_{\mathrm{lv},0}}$	2.392	0.800	0.200
$G_{E_{\mathrm{max,lv}}}$	0.475	0.200	0.200
$k_{\mathrm{E,lv}}$	0.140	0.130	0.110

[a] $E_{\mathrm{max,lv}}$ [mmHg/ml], reference value of the ventricle elastance; $E_{\mathrm{max}_{\mathrm{lv},0}}$ [mmHg/ml], reference value of the ventricle elastance in absence of autoregulation; $G_{E_{\mathrm{max,lv}}}$ [mmHg/ml/(spikes/s)], maximum baroreceptor gain; $k_{\mathrm{E,lv}}$ [1/ml], steepness of the pressure-volume curve.

The conservation of mass and momentum is imposed at each node of the 0-D network through equations analogous to (3). Inertance of the flow is considered only for arterial compartments since in the other elements that term is small with respect to the resistive hydraulic pressure loss and may be neglected. Cardiac valves are considered open if the pressure in the upper chamber is greater than the one in the lower compartment and closed otherwise. In the former case, a nonlinear resistance models the hydraulic pressure loss through the valve. Autoregulation is modeled by differential algebraic equations changing the elastance of the heart ventricles and the resistances and the unstressed reference volumes of splanchnic and extrasplanchnic circulation. Both sympathetic and vagal autoregulation pathways are taken into account[26].

The LVAD is modeled by a pressure-controlled flow generator. Particularly, for each value of the pressure across the device, the corresponding flow is prescribed according to interpolated experimental pressure-flow curves at different rotational speeds[c]. The model has been implemented in Modelica® (a non-proprietary, object-oriented, equation based language aimed at conveniently model complex physical systems[d]) and solved for different device rotational speeds and ventricular elastance corresponding to the case of healthy heart (HH), mid heart failure (MHF), and severe heart failure (SHF); the last two are both in the context of dilated cardiopathy.

To set up the two cases we have changed some of the parameters given in Ursino et al.[26]; these are summarized in Table 1. More precisely, $E_{\mathrm{max,lv}}$ represents the reference value of the ventricle elastance at the instant of maximum contraction for the patient, while $E_{\mathrm{max}_{\mathrm{lv},0}}$ the value in absence of autoregulation, and $G_{E_{\mathrm{max,lv}}}$ the maximum baroreceptor gain (autoregulation effect). By lowering these parameters the contractility properties of

[c] For the data we referred to the HeartMate II® operating manual available at: http://www.thoratec.com.

[d] http://www.modelica.org.

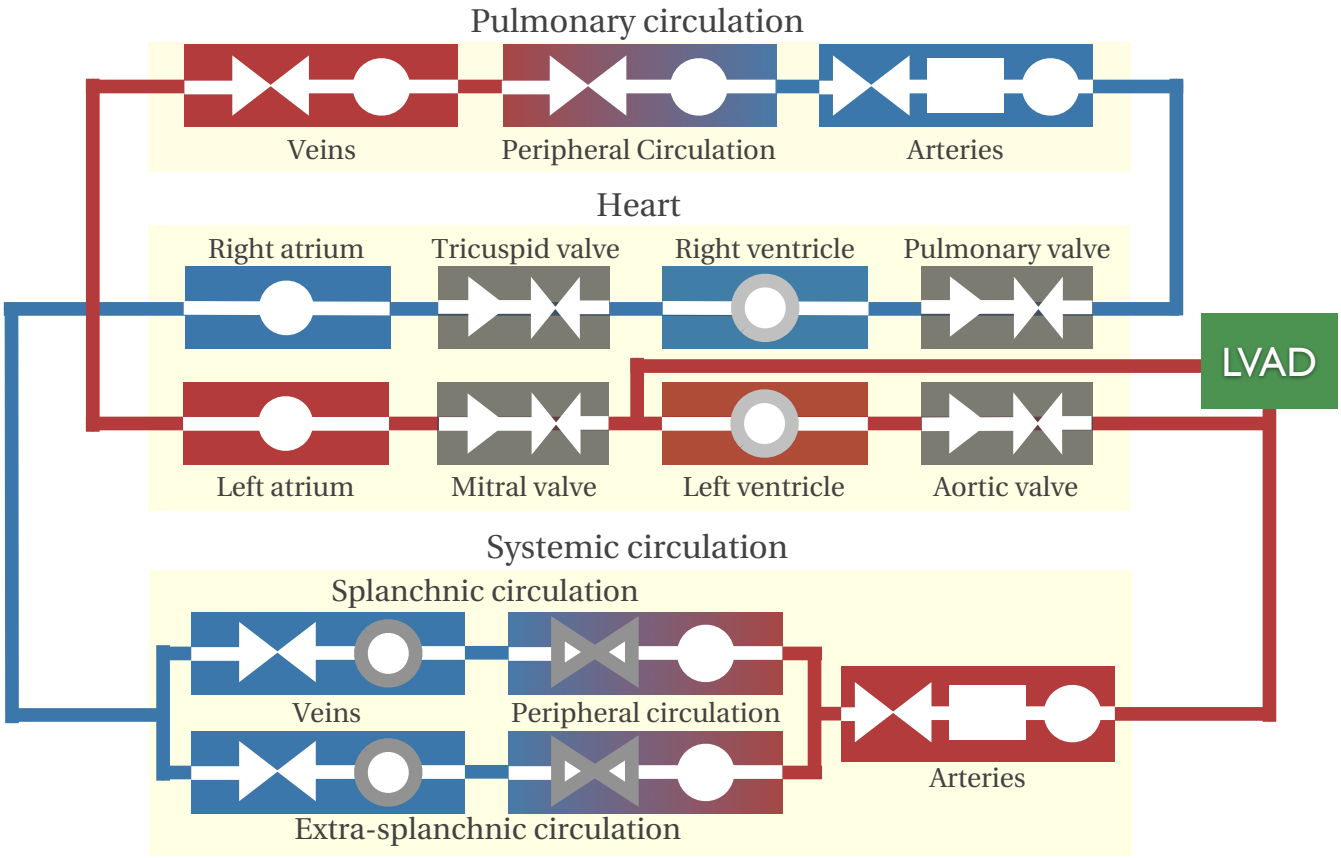

Figure 1: Diagram of the lumped model. Four main compartments may be identified: heart, systemic circulation, and pulmonary circulation. Red elements denote subcompartments containing oxygenated blood while blue elements subcompartment containing deoxygenated blood. White circles represent compliances, white rectangles inertances, and white facing triangles resistances. Single triangles denote proper valves. Elements with a thick gray contour are subject to autoregulation as a function of the arterial pressure at the inlet of the systemic circulation arteries. The LVAD device pump blood from within the left ventricle to the systemic arteries.

the heart are decreased, hence modeling heart failure of different intensity. We also varied $k_{\mathrm{E,lv}}$, the steepness of the pressure-volume curve for the ventricle (supposed to be monoexponential), to be able to correctly represent the pressure-volume curve in patients presenting heart failure of different intensity. All the other parameters are set as in Ursino et al.[26].

3. Lumped parameters model results and validation

In this section we present the numerical results obtained by the lumped parameters model. Particularly, the model offers the possibility to compare and evaluate different scenarios including:

1. different stages of heart failure;
2. pre- and post-operative situations (before and after the device implant);
3. different rotational speeds of the device.

An extensive overview of the results provided by the model is reported in Table 2 for both pre- and post-LVAD implant. Simulations performed without the LVAD aim at comparing the predictive and explanatory ability of the model for the cases described in Section 2, i.e., HH, MHF, and SHF. To set up these simulations we use the parameters reported in Table 1. To validate our results, we compare them with the clinical data given by Cox et al.[41], which are reported in Table 2 under the "Ref." column for the reader's convenience. The values predicted by the model for the case of an healthy heart match the reference data except for the end-systolic volume, which is higher than the upper bound of the clinical range. In the case of middle and severe heart failure the model provides results that are in good agreement with the limits of the clinical ranges for the heart failure (HF), thus representing the case of MHF and SHF. However, in these cases, predicted pulmonary pressures are lower than expected.

Finally the pressure-volume diagrams for the physiological and the two pathological situations are depicted in Fig-

Table 2: Lumped parameter model results with and without LVAD. In the latter case, both model and reference results are provided, where the reference values are clinical data given by Cox et al. [41].

	No VAD					LVAD					
	Ref.		Mod.			8k RPM		9k RPM		10k RPM	
Parameter[b]	HH	HF	HH	MHF	SHF	MHF	SHF	MHF	SHF	MHF	SHF
EF	55-65	15-33	57	32	17	35	17	34	17	33	23
HR	60-100	76-103	71	78	85	75	81	72	77	69	71
EDV	90-162	20-522	133	180	238	169	224	156	208	140	174
ESV	27-45	140-249	56	122	197	110	185	104	172	94	134
LVADPI	-	-	-	-	-	25	15	15	10	10	9
CI	2.8-4.2	1.9-2.4	3.0	2.5	1.9	1.3	0.4	0.7	0.0	0.1	0.0
AQ	-	-	5.4	4.4	3.5	2.2	0.7	1.2	0.0	0.1	0.0
LVADQ	-	-	-	-	-	2.4	3.2	3.7	4.3	5.0	4.9
TOTQ	-	-	5.4	4.4	3.5	4.6	3.9	4.9	4.3	5.1	4.9
SAP	90-140	107-115	131	112	94	109	91	105	89	98	95
DAP	60-90	68-76	88	79	69	83	78	87	84	90	89
MAP	70-105	78-95	102	90	78	92	83	93	85	93	91
SPAP	15-28	54-62	27	30	32	29	30	28	29	27	27
DPAP	5-16	28-29	13	18	23	16	20	15	18	13	14
MPAP	10-22	27-40	18	23	26	21	24	20	22	18	19
PCWP	5-12	17-29	8	14	19	12	17	11	14	8	9

[b] EF [%], ejection factor; HR [1/min], heart rate; EDV [ml], end-diastolic volume; ESV [ml], end-systolic volume; LVADPI, LVAD pulsatile index; CI [L/min/m^2], cardiac index; AQ [L/min], aortic flow rate; LVADQ [L/min], LVAD flow rate; TOTQ [L/min], total flow rate; SAP [mmHg], systolic arterial pressure; DAP [mmHg], diastolic arterial pressure; MAP [mmHg], mean arterial pressure; SPAP [mmHg], systolic pulmonary arterial pressure; DPAP [mmHg], diastolic pulmonary arterial pressure; MPAP [mmHg], mean pulmonary arterial pressure; PCWP [mmHg], pulmonary capillary wedge pressure.

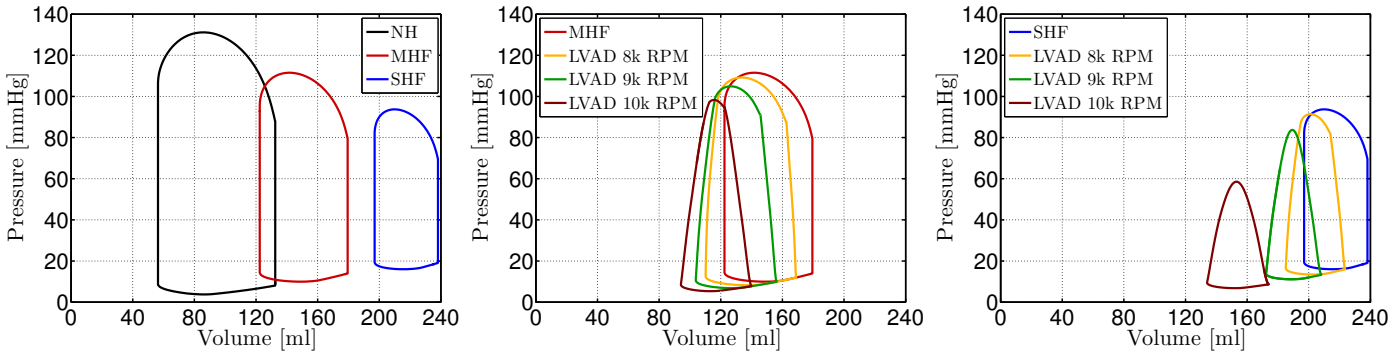

(a) (b) (c)

Figure 2: Comparison of pressure-volume diagrams for several heart conditions and LVAD speeds. (a) Physiological and pathological cases without LVAD. (b) MHF with and without LVAD. (c) SHF with and without LVAD.

ure 2a. The curves for stages of dilated heart failure match both qualitatively and quantitatively the typical curves observed in clinical practice[42]. Note that the pathological conditions, compared to the physiological one, exhibit the presence of systolic dysfunction with increased end-systolic and end-diastolic volumes, decreased stroke volume, and increased end-diastolic pressure.

Configurations including the LVAD were tested for MHF and SHF and for different pump rotational speeds corresponding to the usual values used in the clinical practice (8k, 9k, and 10k RPM). The numerical results show that our model is able, at least qualitatively, to reproduce the main features of the continuous-flow assist devices. Particularly we observe:

1. a flow rate increase when increasing the pump rotational speed;
2. a flow rate increase when decreasing the pressure jump across the pump;
3. a pulsatility decrease when increasing the pump rotational speed (measured by the pulsatile index);
4. a venous pulmonary pressure decrease when increasing the pump rotational speed: this is a well known behavior of LVAD, since it improves pulmonary circulation in patients.

The pressure-volume curves for the middle and severe heart failure states are reported in Figure 2b and Figure 2c, respectively, for different rotational speeds. In all the cases

the device helps in unloading the ventricle from its pumping workload and the effect becomes more evident when the rotational speeds and therefore the LVAD flow rate are increased. The model reproduces the typical triangular pressure volume curves observed in clinical practice for patients under ventricular assistance[43].

In conclusion, the lumped parameters model provides a reliable description of the behavior of the device in different relevant physiological and pathological conditions, since it accounts for the interaction among the ventricle, the assist device, the aorta, and the other parts of the circulatory system. Consequently, it can be used to estimate a proper set of inflow boundary conditions for the network of 1-D arteries. In particular, we generate six sets of boundary data at different values of the rotational speed and for different heart failure levels, as shown in Figure 3 where, for the reader's convenience, the timescale in the images has been normalized to one heart beat; the real timescale can be deduced by the heart rate values reported in Table 2.

The curves exhibit a good qualitative agreement with the experimental data reported, for example, by Khalil et al.[44]. Particularly, the 0-D model allows us to take into account the dynamic interaction between the device and the cardiovascular system itself, predicting, for example, the blood stealing effect that the device has on the ventricle chamber, especially at high rotational speeds. In fact, the device empties the ventricle chamber continuously reducing the amount of blood available to be ejected by the aortic valve during heart contraction. Coherently, the aortic valve flow rate provided by the 0-D model is present only at the systolic phase peak and is reduced by increasing the device RPM, being effectively null in the case of 9k and 10k RPM with SHF. By using the lumped parameters model results as boundary data for the networks of 1-D arteries we take into account these effects.

4. Numerical comparisons of LVAD implant configurations

We use the network of 1-D arteries described in Section 2.1.2 to set up several numerical comparisons between different LVAD implant configurations. The aortic and the LVAD periodic flow rates computed by the lumped parameters model (see Figure 3) are used as inflow boundary data for the network of 1-D arteries, as described in Section 3. Note that these data are supposed to be valid for both the AA and DA cannulations, since the lumped parameters model used was not able to take into account the exact location of the anastomosis. This can introduce a bias in our comparisons by attenuating the differences between AA and DA. We analyze 12 different clinical scenarios obtained by the combination of the two possible sites for the anastomosis of cannula, the two stages of heart failure, and the three available rotational speeds of the device. We remark that not only these scenarios are rather frequent among different patients presenting heart failure, they may also regard a single patient at different stages of the disease, for example in the case of the idiopathic dilated cardiomyopathy in which the device, implanted as a *bridge to recovery*, weans to the progressive full recovery of the heart[4].

The main motivation for our study is to numerically model and compare different sites of outflow cannula anastomosis. Indeed, the network of 1-D arteries allows to perform this analysis by comparing the blood pressures and flow rate wave forms at different locations for the selected clinical scenarios.

In Table 3 we select nine arteries from the global 1-D network and we compare the predicted mean flow rates for the two cannulation techniques. The results show that, regardless of the heart failure stage (MHF or SHF) and rotational speed (8k, 9k, and 10k RPM), the mean flow rate between the AA and DA anastomosis is similar. In particular, the flow rates in the coronaries and in the cerebral arteries for the two approaches may be considered clinically equivalent. This is relevant due to the importance of the heart and cerebral perfusions. Moreover, for all the other arterial segments, the differences between the two approaches have been quantified in less than 1%. Furthermore, we want to assess whether there is any significant difference in the flow rates and pressures wave forms between the two different cannulation techniques. In this respect, we compare the flow rates and pressures wave forms for two limit configurations: the MHF state with LVAD at 8k RPM and the SHF state with LVAD at 10K RPM. In the first case both the cannula and the aortic valve inflows are non-null, such that the systemic circulation is fed from two different points and with flows characterized by different shape and amplitude. In the second case the device is the only flow source since it sucks too much blood from the ventricle for the aortic valve flow rate to be present. Thus the heart does not contribute to the systemic circulation. The results of these comparisons are shown in Figure 4 and Figure 5, respectively. In both configurations, the AA and the DA flow rate and pressure waveforms are almost the same in all the vessels. Finally, in Figure 6 and Figure 7 we show flow rate comparisons at different rotational speeds for the MHF and SHF cases, respectively, in six selected arterial segments. Since the AA and DA cannulations lead to very similar wave forms, in the images we show only the results of the former approach. Similar curves are obtained for the case of the DA cannulation. An increase of the rotational speed of the device decreases the flow rate wave amplitude, regardless of the stage of heart failure. This effect is particularly pronounced in the MHF case in which wave profiles alteration are observed in the right common carotid, in the right vertebral artery, and in the left anterior descending coronary. We recall that loss or reduction of pulsatility and wave profile alterations for flow rates may have adverse effects on human physiology. For this reason, even if numerical simulations have proven that the AA and DA cannulation approaches are similar, particular care should be taken in setting the

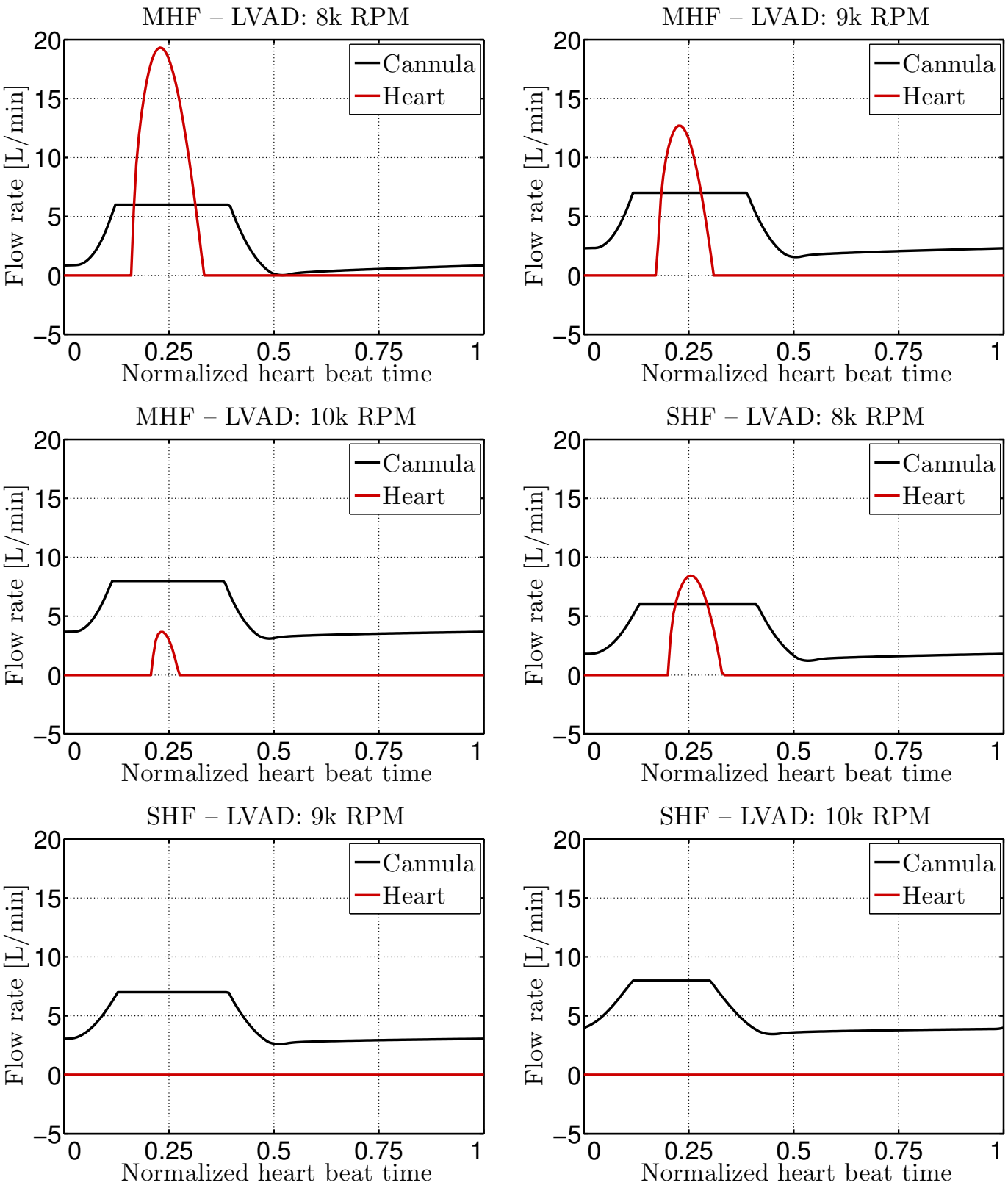

Figure 3: Time dependent inflow boundary conditions for the 1-D arterial network computed with the lumped parameters model as a function of the LVAD rotational speed and of the heart failure level.

correct device rotational speed.

Table 3: Mean flow rate comparison, at several location of the arterial network, between different LVAD configurations and heart failures. The flow rates are expressed in [ml/s].

	MHF [RPM]						SHF [RPM]					
	8k		9k		10k		8k		9k		10k	
Location	AA	DA	AA	DA	AA	DA	AA	DA	AA	DA	AA	DA
Abdominal aorta	40.822	40.880	42.715	42.783	44.798	44.849	34.596	34.665	37.719	37.776	43.160	43.208
Left main coronary	3.215	3.210	3.356	3.349	3.507	3.500	2.751	2.746	2.979	2.973	3.382	3.376
Left ant. desc. coron.	1.532	1.530	1.599	1.596	1.673	1.669	1.309	1.307	1.418	1.415	1.612	1.609
Right coronary RCA	1.346	1.344	1.407	1.404	1.472	1.469	1.146	1.143	1.244	1.242	1.418	1.416
Right common carotid	4.123	4.101	4.322	4.297	4.528	4.508	3.483	3.460	3.798	3.779	4.356	4.341
Right vertebral	0.891	0.886	0.920	0.913	0.949	0.941	0.815	0.808	0.856	0.849	0.927	0.919
Left subclavian	4.289	4.298	4.522	4.533	4.763	4.772	3.632	3.642	3.998	4.007	4.599	4.605
Right renal	8.821	8.825	9.219	9.225	9.651	9.656	7.509	7.515	8.157	8.162	9.298	9.303
Right common iliac	5.521	5.520	5.771	5.772	6.059	6.061	4.629	4.629	5.062	5.064	5.826	5.831
Right anterior tibial	0.940	0.939	0.977	0.977	1.022	1.022	0.778	0.778	0.848	0.848	0.980	0.980

5. Limitations and extension of the current work

Our model proved to be effective in describing the global cardiovascular response to the implant of a LVAD, to its location, and to its rotational speed. However, the present work presents some limitations that should be further investigated in the future. Being based on reduced dimensional techniques which provide only spatial averages of the quantities of interest, our approach neglects possibly relevant 3-D effects like vortex flow regions, turbulent flow regions, zones of stagnation, and abnormal distributions of the wall shear stress at the site of anastomosis or at vessels bifurcations. These flow patterns can, in principle, lead to complications, e.g., thrombosis or hemolysis, to long-term effect on aortic wall, i.e., remodeling, or to haemodynamical effects on the aortic valve, i.e., valve regurgitation. These limitations could be partly overcome using a 3-D model of the cannula anastomosed to the aorta, thus considering the 3-D dynamics of the flow in that region[45].[45]. The use of 3-D geometries, besides allowing the study of the effect of the site and the angle of the anastomosis of the cannula, make it possible a comparison of 3-D flow patterns with data from the literature[13].

Another limitation of the present work is that the 0-D and the 1-D model do not provide reciprocal feedbacks, being effectively decoupled. In fact the lumped parameters model is used only to pre-generate the inflow boundary condition for the cannula while the 1-D model does not feature a closed loop as it only accounts for the description of the systemic arteries. In this respect, the development of a closed-loop model which accounts for the interaction between a detailed (i.e., 1-D plus 3-D) systemic circulation and a lumped description of the peripheral and venous compartments, as well as of the LVAD pump, may provide more accurate results. Another possible extension of the present model deals with the inclusions of the effects due to nonlinear material properties of blood and wall tissues. However, these effects are generally considered negligible when using reduced order models, such as the 1-D FSI model employed in this work. More precisely, the assumption of a linear elastic stress-strain wall relation is acceptable unless specific clinical scenarios dominated by the nonlinear mechanics of the wall are analyzed (e.g., stenoses or aneurysms); for this class of problems, a 3-D description of the flow and of the arterial wall could be essential.

6. Conclusions

In this work we developed a geometrical multiscale model to simulate the interaction of a LVAD with the systemic circulation. A brief description of the employed models including some details about the used numerical approximation have been provided. Our work had three main goals.

1. The development of a multiscale framework for assessing the cardiovascular response to the implant of a LVAD. This framework effectively combines a lumped mathematical model with autoregulation and a network of 1-D FSI arteries that in future works can be extended to include local 3-D blocks. The lumped parameters model has been validated for different stages of heart failure and is able to represent different clinical situations pre- and post-LVAD implant, being therefore able to provide reliable preliminary results on pressures and flow rates, accounting for the interaction between the device and the global circulation. The 1-D FSI arteries model uses the results of the lumped model as inflow boundary data and provides an effective description of the flow rates and pressure in the global arterial tree. Through this framework we were able to study several clinical scenarios, given by the combination of two possible sites for the anastomosis of cannula of the LVAD (AA and DA), three rotational speed of the device (8k, 9k, and 10k RPM), and two stages of heart failure (MHF and SHF).
2. The assessment of possible difference in flow rates and pressure patterns depending on the location of the anastomosis. In this respect the results for AA and

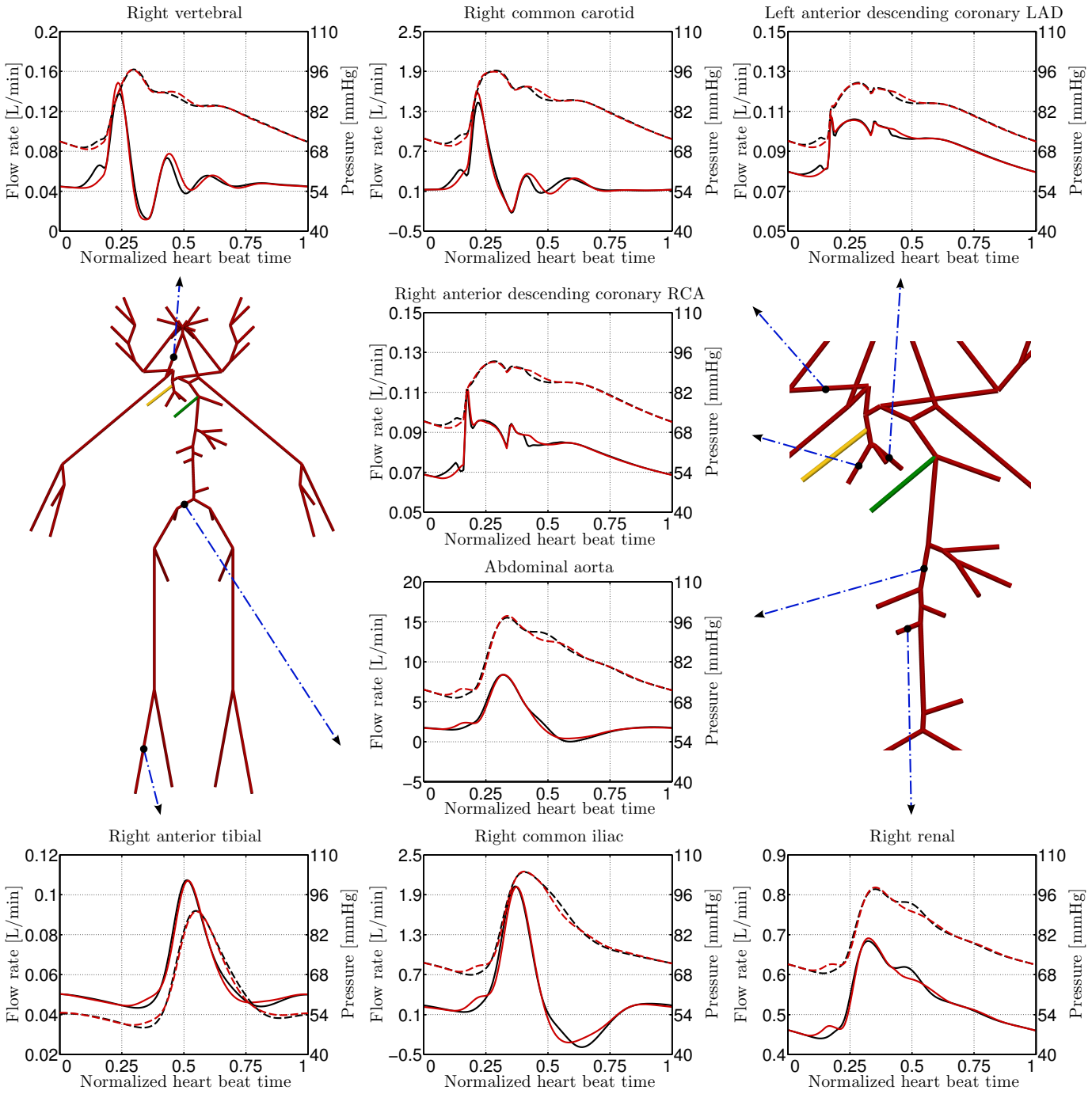

Figure 4: Flow rate (solid lines) and pressure (dashed lines) comparison between AA (black lines) and DA (red lines) cannula configurations in eight different arterial vessels for a MHF with LVAD at 8k RPM. The left image represents a global view of the 1-D network elements, while the right one is a zoomed view of the aortic region. The yellow and green segments represent the two configurations for the cannula (AA and DA, respectively). Positioning of the elements is purely visual.

DA cannulations exhibit similar wave forms and mean flow rates in all the considered cases. In spite of the limitations of our model, the results confirmed that, as mentioned in Section 1, DA cannulation remains an adequate therapeutic option, especially in patients who are at high risk for the AA cannulation.

3. The assessment of possible difference in flow rates and pressure patterns depending on rotational speed of the device. In this respect the results show that, regardless of the anastomosis region, the rotational speed of the device has a significant impact on the wave profiles. In particular, the pulsatility decreases by in-

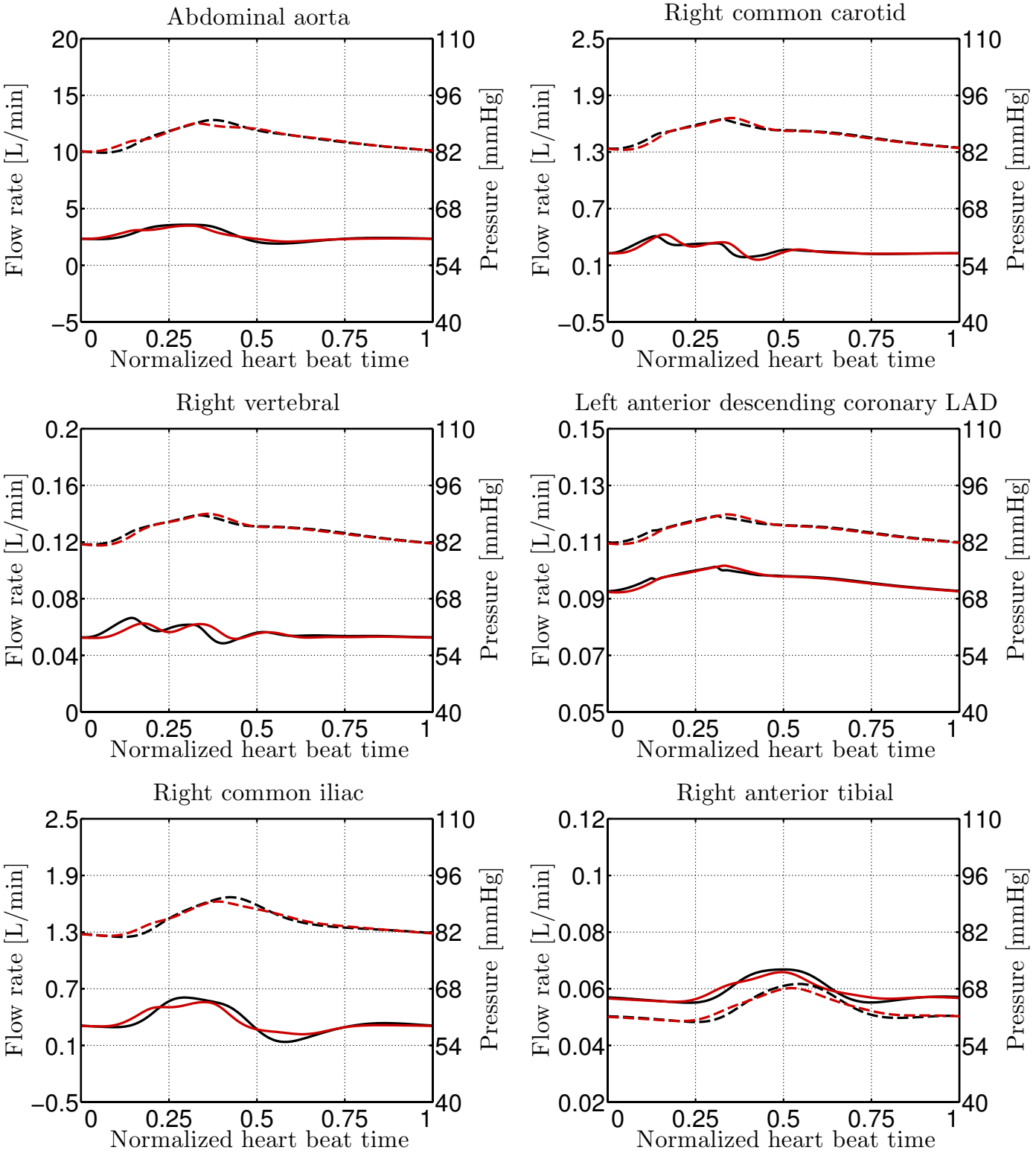

Figure 5: Flow rate (solid lines) and pressure (dashed lines) comparison between AA (black lines) and DA (red lines) cannula configurations in six different arterial vessels for a SHF with LVAD at 10k RPM.

creasing the rotational speed of the device and this effect is more pronounced at high RPM. The resulting continuous-flow physiology is a well known issue of these devices, for which the clinical impact is still not clear, even if it is suspected to be relevant especially in the long term period. Indeed, manufacturers are now trying to re-introduce pulsatility in continuous-flow devices by, e.g., varying the RPM in time. From

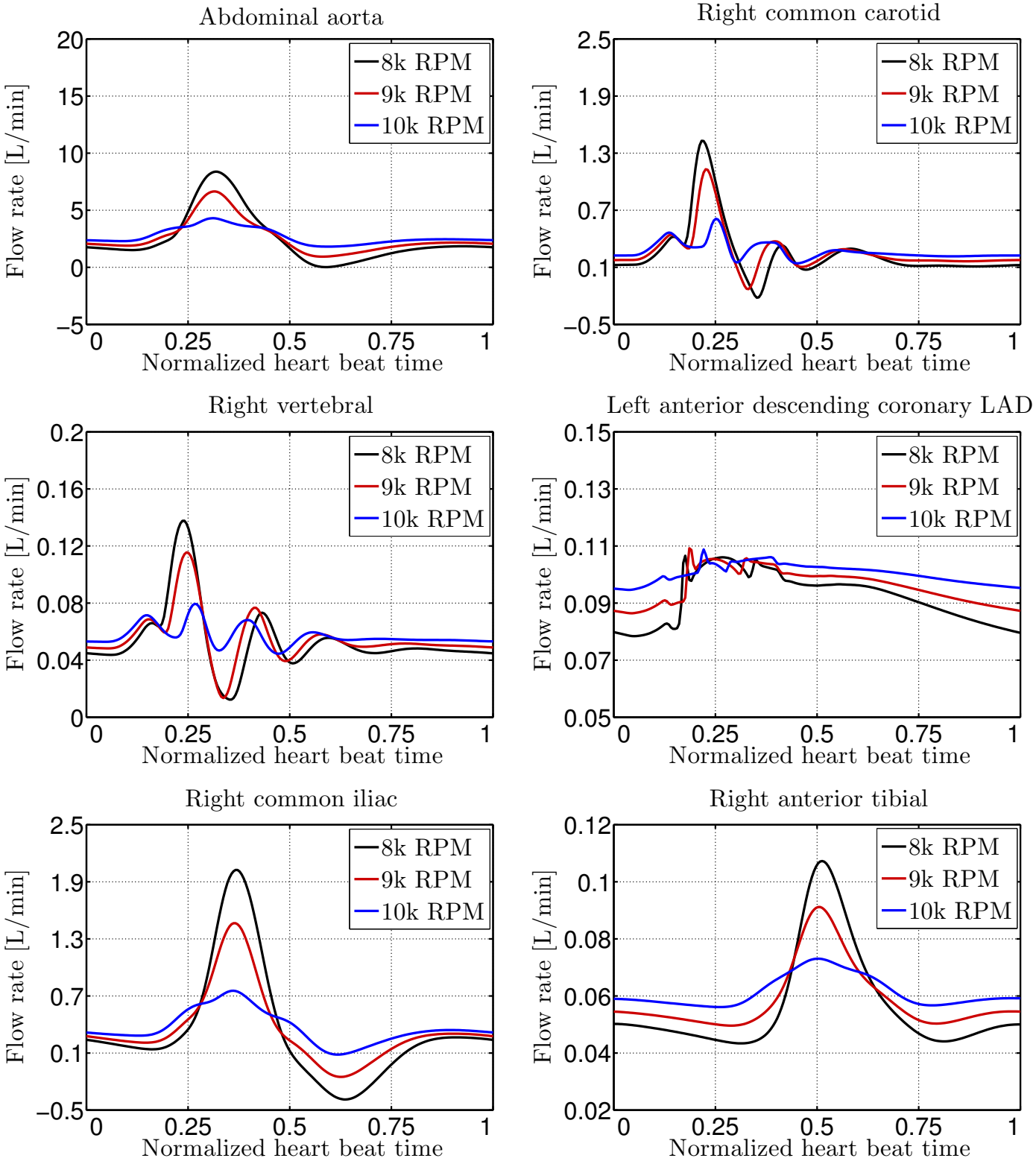

Figure 6: Flow rate comparison, in six different arterial vessels, for three different speed of the LVAD anastomoted to the AA of a patient with MHF.

this viewpoint this model might be useful to evaluate and test new devices and functioning modes.

Although the current model presents some limitations (see Section 5), our mathematical framework has proven to be effective in describing and capturing many global phenom-

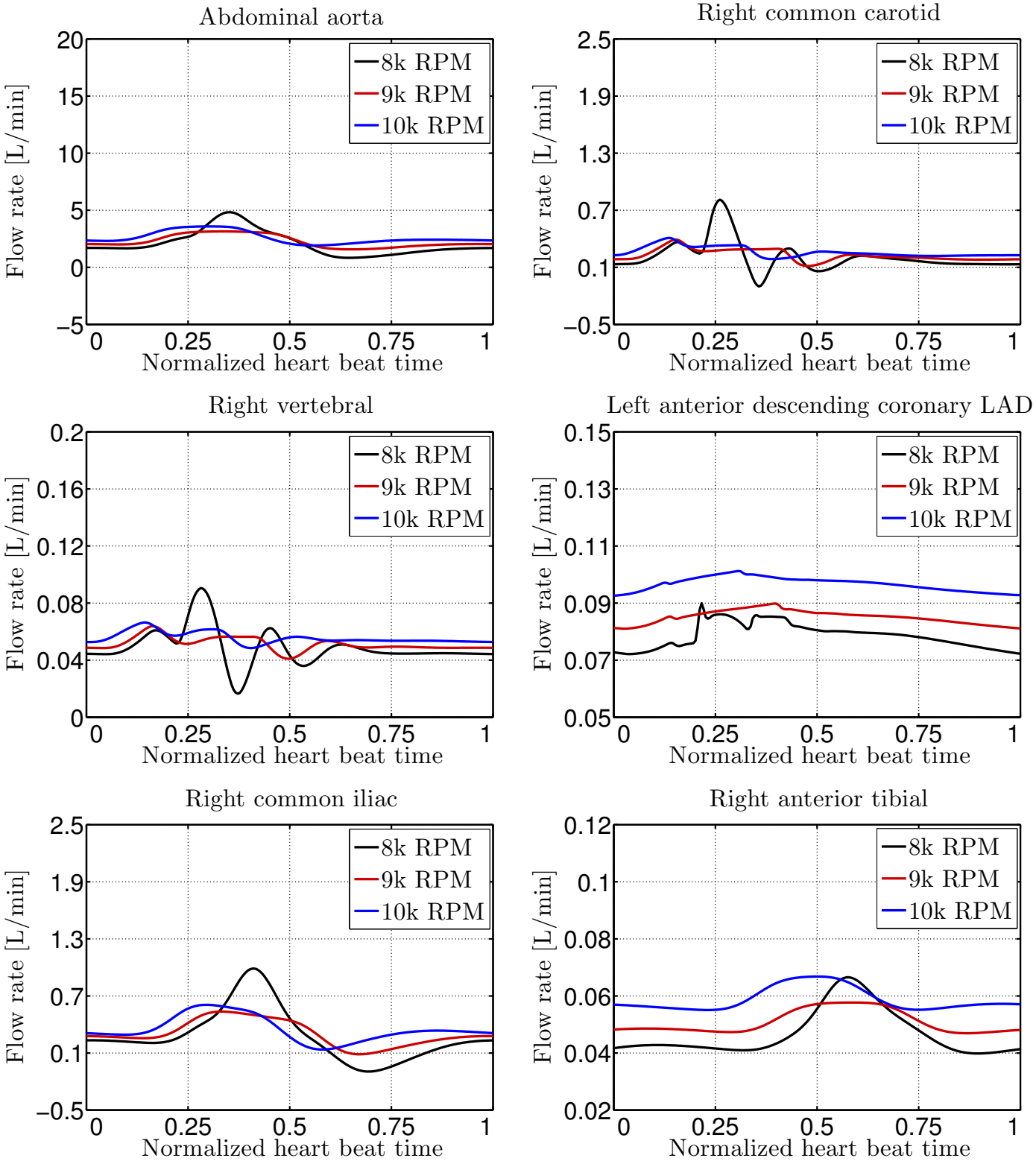

Figure 7: Flow rate comparison, in six different arterial vessels, for three different speed of the LVAD anastomoted to the AA of a patient with SHF.

ena and, in spite of neglecting specific local 3-D flow patterns, it provides indication that may be considered already useful in clinical practice. Moreover, the introduced multiscale framework could easily be extended to include local 3-D geometries. To conclude, in future studies the geometrical multiscale model will be used to evaluate sev-

eral new clinical scenarios. For example, for the evaluation of the hemodynamic response and pump behavior in aortic regurgitation, which is a common problem, or for testing different devices under typical clinical situations.

Acknowledgements

J. Bonnemain acknowledges the Swiss National Fund (SNF) grant 323630-133898. A. C. I. Malossi acknowledges the Swiss Platform for High-Performance and High-Productivity Computing (HP2C). We also acknowledge the European Research Council Advanced Grant "Mathcard, Mathematical Modelling and Simulation of the Cardiovascular System", Project ERC-2008-AdG 227058. This work was also supported by a grant from the Swiss National Supercomputing Centre (CSCS) under project ID s190. The 1-D network simulations presented in this paper have been computed using the `LifeV` library (www.lifev.org).

Conflict of Interest

There are no conflict of interest to declare.

Ethical Approval

Not required.

References

[1] C. A. Thunberg, B. D. Gaitan, F. A. Arabia, D. J. Cole, A. M. Grigore, Ventricular assist devices today and tomorrow, J. Cardiothorac. Vasc. Anesth. 24 (2010) 656–680.

[2] V. L. Roger, A. S. Go, D. M. Lloyd-Jones, R. J. Adams, J. D. Berry, T. M. Brown, M. R. Carnethon, S. Dai, G. de Simone, E. S. Ford, et al., Heart disease and stroke statistics – 2011 update: A report from the American Heart Assiciation, Circulation 123 (2011) e18–e209.

[3] L. W. Miller, F. D. Pagani, S. D. Russell, R. John, A. J. Boyle, K. D. Aaronson, J. V. Conte, Y. Naka, D. Mancini, R. M. Delgado, et al., Use of a continuous-flow device in patients awaiting heart transplantation, N. Engl. J. Med. 357 (2007) 885–896.

[4] E. J. Birks, P. D. Tansley, J. Hardy, R. S. George, C. T. Bowles, M. Burke, N. R. Banner, A. Khaghani, M. H. Yacoub, Left ventricular assist device and drug therapy for the reversal of heart failure, N. Engl. J. Med. 355 (2006) 1873–1884.

[5] E. A. Rose, A. C. Gelijns, A. J. Moskowitz, D. F. Heitjan, L. W. Stevenson, W. Dembitsky, J. W. Long, D. D. Ascheim, A. R. Tierney, R. G. Levitan, et al., Long-term mechanical left ventricular assistance for end-stage heart failure, N. Engl. J. Med. 345 (2001) 1435–1443.

[6] E. A. Ziemba, R. John, Mechanical circulatory support for bridge to decision: Which device and when to decide, J. Card. Surg. 25 (2010) 425–433.

[7] S. Westaby, O. H. Frazier, D. W. Pigott, S. Saito, R. K. Jarvik, Implant technique for the Jarvik 2000 heart, Ann. Thorac. Surg. 73 (2002) 1337–1340.

[8] O. H. Frazier, I. D. Gregoric, W. E. Cohn, Initial experience with non-thoracic, extraperitoneal, off-pump insertion of the Jarvik 2000 heart in patients with previous median sternotomy, J. Heart Lung Transplant. 25 (2006) 499–503.

[9] K. N. Litwak, S. C. Koenig, H. Tsukui, S. I. Kihara, Z. Wu, G. M. Pantalos, Effects of left ventricular assist device support and outflow graft location upon aortic blood flow, ASAIO J. 50 (2004) 432–437.

[10] K. N. Litwak, S. C. Koenig, R. C. Cheng, G. A. Giridharan, K. J. Gillars, G. M. Pantalos, Ascending aorta outflow graft location and pulsatile ventricular assist provide optimal hemodynamic support in an adult mock circulation, Artif. Organs 29 (2005) 629–635.

[11] P. L. DiGiorgi, D. L. Smith, Y. Naka, M. C. Oz, In vitro characterization of aortic retrograde and antegrade flow from pulsatile and non-pulsatile ventricular assist devices, J. Heart Lung Transplant. 23 (2004) 186–192.

[12] K. Nawata, T. Nishimura, S. Kyo, M. Hisagi, O. Kinoshita, A. Saito, N. Motomura, S. Takamoto, M. Ono, Outcomes of midterm circulatory support by left ventricular assist device implantation with descending aortic anastomosis, J. Artif. Organs 13 (2010) 197–201.

[13] Y. Bazilevs, J. R. Gohean, T. J. R. Hughes, R. D. Moser, Y. Zhang, Patient-specific isogeometric fluid-structure interaction analysis of thoracic aortic blood flow due to implantation of the Jarvik 2000 left ventricular assist device, Comp. Meth. Appl. Mech. Engrg. 198 (2009) 3534–3550.

[14] O. H. Frazier, T. J. Myers, I. D. Gregoric, T. Khan, R. Delgado, M. Croitoru, K. Miller, R. Jarvik, S. Westaby, Initial clinical experience with the Jarvik 2000 implantable axial-flow left ventricular assist system, Circulation 105 (2002) 2855–2860.

[15] E. Tuzun, C. Narin, I. D. Gregoric, W. E. Cohn, O. H. Frazier, Ventricular assist device outflow-graft site: effect on myocardial blood flow, J. Sur. Res. 171 (2011) 71–75.

[16] A. Ghodsizad, B. J. Kar, P. Layolka, A. Okur, J. Gonzales, C. Bara, M. N. Ungerer, M. Karck, I. D. Gregoric, A. Ruhparwar, Less invasive off-pump implantation of axial flow pumps in chronic ischemic heart failure: Survival effects, J. Heart Lung Transplant. 30 (2011) 834–837.

[17] K. May-Newman, B. Hillen, W. Dembitsky, Effect of left ventricular assist device outflow conduit anastomosis location on flow patterns in the native aorta, ASAIO J. 52 (2006) 132–139.

[18] N. Yang, S. Deutsch, E. G. Paterson, K. B. Manning, Numerical study of blood flow at the end-to-side anastomosis of a left ventricular assist device for adult patients, J. Biomech. Eng. 131 (2009) 111005.

[19] N. Yang, S. Deutsch, E. G. Paterson, K. B. Manning, Hemodynamics of an end-to-side anastomotic graft for a pulsatile pediatric ventricular assist device, J. Biomech. Eng. 132 (2010) 031009.

[20] B. Kar, R. M. Delgado, O. H. Frazier, I. D. Gregoric, M. T. Harting, Y. Wadia, T. J. Myers, R. D. Moser, J. Freund, The effect of LVAD aortic outflow-graft placement on hemodynamics and flow: Implantation technique and computer flow modeling, Tex. Heart Inst. J. 32 (2005) 294–298.

[21] M. R. Noor, C. Bowles, N. R. Banner, Relationship between pump speed and exercise capacity during HeartMate II left ventricular assist device support: influence of residual left ventricular function, Eur. J. Heart Fail. 14 (2012) 613–620.

[22] P. Brassard, A. S. Jensen, N. Nordsborg, F. Gustafsson, J. E. Møller, C. Hassager, S. Boesgaard, P. B. Hansen, P. S. Olsen, K. Sander, N. H. Secher, P. L. Madsen, Central and peripheral blood flow during exercise with a continuous-flow left ventricular assist device, Circ. Heart Fail. 4 (2011) 554–560.

[23] A. C. I. Malossi, P. J. Blanco, S. Deparis, A. Quarteroni, Algorithms for the partitioned solution of weakly coupled fluid models for cardiovascular flows, Int. J. Num. Meth. Biomed. Engng. 27 (2011) 2035–2057.

[24] A. C. I. Malossi, P. J. Blanco, S. Deparis, A two-level time step technique for the partitioned solution of one-dimensional arterial networks, Comp. Meth. Appl. Mech. Engrg. 237–240 (2012) 212–226.

[25] P. Reymond, F. Merenda, F. Perren, D. Rüfenacht, N. Stergiopulos, Validation of a one-dimensional model of the systemic arterial tree, Am. J. Physiol. Heart Circ. Physiol. 297 (2009)

H208–H222.

[26] M. Ursino, Interaction between carotid baroregulation and the pulsating heart: a mathematical model, Am. J. Physiol. Heart Circ. Physiol. 275 (1998) H1733–H1747.

[27] A. P. Avolio, Multi-branched model of the human arterial system, Med. Biol. Engrg. Comp. 18 (1980) 709–718.

[28] N. Stergiopulos, D. F. Young, T. R. Rogge, Computer simulation of arterial flow with applications to arterial and aortic stenoses, J. Biomech. 25 (1992) 1477–1488.

[29] M. S. Olufsen, Modeling the arterial system with reference to an anesthesia simulator, Ph.D. thesis, Roskilde University, 1998.

[30] L. Formaggia, D. Lamponi, A. Quarteroni, One-dimensional models for blood flow in arteries, J. Eng. Math. 47 (2003) 251–276.

[31] F. Liang, H. Liu, A closed-loop lumped parameter computational model for human cardiovascular system, JSME International Journal 48 (2005) 484–493.

[32] J. Alastruey, K. H. Parker, J. Peiró, S. M. Byrd, S. J. Sherwin, Modelling the circle of Willis to assess the effects of anatomical variations and occlusions on cerebral flows, J. Biomech. 40 (2007) 1794–1805.

[33] P. J. Blanco, J. S. Leiva, R. A. Feijóo, G. C. Buscaglia, Black-box decomposition approach for computational hemodynamics: One-dimensional models, Comp. Meth. Appl. Mech. Engrg. 200 (2011) 1389–1405.

[34] N. Stergiopulos, B. Westerhof, N. Westerhof, Total arterial inertance as the fourth element of the windkessel model, Am. J. Physiol. 276 (1999) H81–H88.

[35] P. Segers, N. Stergiopulos, N. Westerhof, P. Wouters, P. Kolh, P. Verdonck, Systemic and pulmonary hemodynamics assessed with a lumped-parameter heart-arterial interaction model, J. Eng. Math. 47 (2003) 185–199.

[36] V. Milišić, A. Quarteroni, Analysis of lumped parameter models for blood flow simulations and their relation with 1D models, ESAIM: Mathematical Modelling and Numerical Analysis 38 (2004) 613–632.

[37] J. T. Ottesen, M. S. Olufsen, J. K. Larsen, Applied Mathematical Models in Human Physiology, volume MM09 of *Monographs on Mathematical Modeling and Computation*, SIAM, 2004.

[38] E. Lanzarone, P. Liani, G. Baselli, M. L. Constantino, Model of arterial tree and peripheral control for the study of physiological and assisted circulation, Med. Eng. Phys. 29 (2007) 542–555.

[39] Y. Shi, P. Lawford, R. Hose, Review of Zero-D and 1-D models of blood flow in the cardiovascular system, BioMedical Engineering OnLine 10 (2011) 1–38.

[40] L. Formaggia, A. Quarteroni, A. Veneziani, Cardiovascular Mathematics, volume 1 of *Modeling, Simulation & Applications*, Springer-Verlag, Milan, 2009.

[41] L. G. E. Cox, S. Loerakker, M. C. M. Rutten, B. A. J. M. de Mol, F. N. van de Vosse, A mathematical model to evaluate control strategies for mechanical circulatory support, Artif. Organs 33 (2009) 593–603.

[42] N. Westerhof, N. Stergiopulos, M. I. M. Noble, Snapshots Of Hemodynamics: An Aid For Clinical Research And Graduate Education, Basic Science for the Cardiologist, Springer-Verlag, 2nd edition, 2010.

[43] S. C. Koenig, G. M. Pantalos, K. J. Gillars, D. L. Ewert, K. N. Litwak, S. W. Etoch, Hemodynamic and pressure-volume responses to continuous and pulsatile ventricular assist in an adult mock circulation, ASAIO J. 50 (2004) 15–24.

[44] H. A. Khalil, W. E. Cohn, R. W. Metcalfe, O. H. Frazier, Preload sensitivity of the Jarvik 2000 and HeartMate II left ventricular assist devices, ASAIO J. 54 (2008) 245–248.

[45] J. Bonnemain, S. Deparis, A. Quarteroni, Connecting ventricular assist devices to the aorta: a numerical model, in: Imagine Math. Between Culture and Mathematics, Springer-Verlag, 2012, pp. 211–224.

Recent publications :

MATHEMATICS INSTITUTE OF COMPUTATIONAL SCIENCE AND ENGINEERING
Section of Mathematics
Ecole Polytechnique Fédérale
CH-1015 Lausanne

07.2012 J BONNEMAIN, S. DEPARIS, A. QUARTERONI:
Connecting ventricular assist devices to the aorta: a numerical model

08.2012 J BONNEMAIN, ELENA FAGGIANO, A. QUARTERONI, S. DEPARIS:
A framework for the analysis of the haemodynamics in patient with ventricular assist device

09.2012 T. LASSILA, A. MANZONI, G. ROZZA:
Reduction strategies for shape dependent inverse problems in haemodynamics

10.2012 C. MALOSSI, P. BLANCO, P. CROSETTO, S. DEPARIS, A. QUARTERONI:
Implicit coupling of one-dimensional and three-dimensional blood flow models with compliant vessels

11.2012 S. FLOTRON J. RAPPAZ:
Conservation schemes for convection-diffusion equations with Robin's boundary conditions

12.2012 A. UMSCHMAJEW, B. VANDEREYCKEN:
The geometry of algorithms using hierarchical tensors

13.2012 D. KRESSNER, B. VANDEREYCKEN:
Subspace methods for computing the pseudospectral abscissa and the stability radius

14.2012 B. JEURIS, R. VANDEBRIL, B. VANDEREYCKEN:
A survey and comparison of contemporary algorithms for computing the matrix geometric mean

15.2012 A. MANZONI, A. QUARTERONI, G. ROZZA:
Computational reduction for parametrized PDEs: strategies and applications

16.2012 A.C.I. MALOSSI, J. BONNEMAIN:
Numerical comparison and calibration of geometrical multiscale models for the simulation of arterial flows

17.2012 A. ABDULLE, W. E, B. ENGQUIST, E. VANDEN-EIJNDEN:
The heterogeneous multiscale method

18.2012 D. KRESSNER, M. PLESINGER, C. TOBLER:
A preconditioned low-rank CG method for parameter-dependent Lyapunov matrix equations

19.2012 A. MANZONI, T. LASSILA, A. QUARTERONI, G. ROZZA:
A reduced-order strategy for solving inverse Bayesian shape identification problems in physiological flows

20.2012 J. BONNEMAIN. C. MALOSSI, M. LESINIGO, S. DEPARIS, A. QUARTERONI, L. VON SEGESSER:
Numerical simulation of left ventricular assist device implantations: comparing the ascending and descending aorta cannulations